Evidence for Forcing-Dependent Steady States in a Turbulent Swirling Flow

B. Saint-Michel,[1,*] B. Dubrulle,[1] L. Marié,[2] F. Ravelet,[3] and F. Daviaud[1]

[1]*Laboratoire SPHYNX, Service de Physique de l'État Condensé, DSM, CEA Saclay, CNRS URA 2464, 91191 Gif-sur-Yvette, France*
[2]*Laboratoire de Physique des Océans, UMR 6523 CNRS/IFREMER/IRD/UBO, 29285 Brest, France*
[3]*Laboratoire Dynfluid, ENSAM ParisTech, CNRS EA92, 151, boulevard de l'Hôpital 75013 Paris, France*

(Received 9 January 2013; published 4 December 2013)

We study the influence on steady turbulent states of the forcing in a von Karman flow, at constant impeller speed, or at constant torque. We find that the different forcing conditions change the nature of the stability of the steady states and reveal dynamical regimes that bear similarities to low-dimensional systems. We suggest that this forcing dependence may be applicable to other turbulent systems.

DOI: 10.1103/PhysRevLett.111.234502 PACS numbers: 47.20.Ky, 05.45.−a, 47.27.Sd

Introduction.—Turbulence is a feature common to almost all natural flows. Yet, their large size and complex forcing or boundary conditions make them out-of-reach of exact description using, e.g., direct numerical simulation. Their modelling, therefore, relies upon a classical paradigm: at a large enough Reynolds number, and in a suitable range of scale—the inertial range—any turbulent flow reaches a ''universal'' regime independent of large scale forcing and small scale dissipation processes, allowing characterization in laboratory experiments or numerical simulations. This paradigm has, however, been challenged by the observations that the influence of intrinsic large scale anisotropy, very frequent in natural flows, actually decreases much slower than predicted by simple dimensional analysis. Thus, a universal regime can only be achieved if anisotropic fluctuations are subleading (for a review, see, e.g., [1]). Another way to question the paradigm is through the forcing mechanism. In natural flows, forcing is achieved through constant flux conditions: heat flux through solar radiation in the atmosphere, momentum flux through wind at the ocean surface. In laboratory or direct numerical simulation, it is often more convenient to force through either a body force, or constant temperature, or velocity condition, i.e., via the conjugate quantity with respect to total power injection. The question of whether two conjugate forcings will produce the same steady states is highly nontrivial: for example, in the simple case of statistical physics of systems displaying long range interactions, equilibrium solutions in the microcanonical (''energy constrained'') ensemble are not necessarily equilibrium solutions in the canonical (''temperature constrained'') ensemble [2,3], a property named ensemble inequivalence. Exploring the steady state stability in (out-of-equilibrium) turbulent flows may, therefore, be seen as a natural extension of this concept, with high relevance to geophysical flows modelling.

In this Letter, we use a controlled laboratory experiment, a von Kármán swirling flow. It consists of a cylinder of fluid stirred by two counter-rotating impellers, producing fully developed turbulence in a small experimental device. When forced under stable conditions, steady states are established, that have been successfully compared with equilibrium solutions of the axisymmetric Euler equations [4]. The steady states are nonunique [5] and may experience spontaneous symmetry breaking with diverging susceptibility [6]. In this Letter, we examine the stability of such steady states under two different, conjugate forcing conditions, either imposing the speed or the torque—flux of angular momentum [7]—to our impellers. The subject has attracted little attention, work focusing on the difference of global power fluctuations [8–10] under both conditions. However, switching from speed to torque control is shown to alter the stability of the steady states previously observed in [5] and to reveal interesting dynamical regimes.

Experimental setup.—The von Kármán flow is created in a polycarbonate cylinder of radius $R = 100$ mm filled with water. The fluid is stirred by two impellers of radius $0.925R$ fitted with eight curved blades. The impellers are separated from each other by a distance $1.4R$. Two independent 1.8 kW brushless motors can rotate the impellers either by imposing their speeds (f_1, f_2) or their torques (C_1, C_2). Torque and speed measurements are performed by two Scaime MR12 torque sensors fixed to the mechanical shafts driving the impellers. Fluid confinement is assured by two balanced mechanical seals under a 2.8 bar pressure to provide minimum friction. Temperature is regulated by an external water flow in two refrigeration coils installed behind each impeller. The typical Reynolds number, defined as $\mathrm{Re} = \pi(f_1 + f_2)R^2/\nu$, and varying from 2×10^5 to 5×10^5, is well above the transition to turbulence reported in [11].

Our experiments aim to measure the flow response to asymmetric forcing for both types of controls. Speed control experiments will impose $(f_1 + f_2)/2 = 4$ Hz to study the influence of $f_1 \neq f_2$ on the values of C_1 and C_2. Reciprocally, torque control fixes $(C_1 + C_2)/2 = 1.40$ Nm to study the effect of torque asymmetries on the impeller speeds f_1 and f_2. The upside-down $\mathcal{R}_\pi$ symmetry (see inset in Fig. 1) provides a definition of two

antisymmetric dimensionless quantities θ and γ to measure the forcing—and response—asymmetry: $\theta = (f_1 - f_2)/(f_1 + f_2)$ is the reduced impeller speed difference and $\gamma = (C_1 - C_2)/(C_1 + C_2)$ is the reduced shaft torque difference.

Speed control.—For speed-imposed experiments, all turbulent flows are steady. These steady states are characterized by their mean torque asymmetry γ. Starting both impellers at the same time for $\theta \approx 0$, the system reaches steady states corresponding to a "symmetric" branch called (s). They statistically consist of two recirculation cells separated by a shear layer, in agreement with [5,6]. In such states, a small θ variation triggers a transition with a dramatic increase of the mean torque. These new "bifurcated" states exhibit one recirculation cell, and form two separate branches of the (γ, θ) plane (see Fig. 1, left). These branches, named (b_1) and (b_2), respectively, exhibit a global pumping of the bottom or the top impeller. Velocimetry measurements have confirmed that the velocity fields of the flows belonging to the (b_1) and (b_2) are images of each other by the $\mathcal{R}_\pi$ rotation. Once on (b_1) and (b_2) branches, the (s) state cannot be reached, which is, therefore, marginally stable. In addition, the (b_1) and (b_2) branches are hysteretic, (b_1) states persisting for $f_1 \leq f_2$ and (b_2) states for $f_2 \leq f_1$ [12], agreeing with previous results [5]. The shape of the hysteresis cycle is only weakly Reynolds-dependent for $\mathrm{Re} \geq 1.0 \times 10^5$, as evidenced by water and liquid helium experiments performed up to $\mathrm{Re} = 3.0 \times 10^8$ [13]. An important feature of the cycle is the "forbidden zone" of γ values never accessed for imposed speed.

Torque control.—In contrast, imposing torque allows any value of γ, assuming friction is negligible, whereas f is no longer fixed. Hence, with our definition, we cannot specify *a priori* the Reynolds number of such experiments. We have first verified that imposing γ out of the forbidden zone provides steady states identical to those observed in speed control (see Fig. 1). After suitable normalization, no difference in velocimetry measurements is indeed observed between the two controls. Our experiments have then focused on the henceforth accessible forbidden zone. In this region, the system loses steadiness: the impeller speed may alternatively jump between multiple attracting turbulent states. This multistability is identified by the emergence of multiple local maxima in the probability density function (PDF) of the 1.5 Hz low-pass filtered signal of $\theta(t)$. Such filtering is required considering the discrete nature of our speed measurements; it yields a robust density function when the filter cutoff frequency is changed. Three types of attracting states, then, have been identified: $(\tilde{s})$, the high-speed state, is similar to (s); $(\tilde{b_1})$ and $(\tilde{b_2})$ are low-speed states similar to (b_1) and (b_2); and two new $(\tilde{i_1})$ and $(\tilde{i_2})$ intermediate states. These new states can be seen in Fig. 1: while $(\tilde{s})$, $(\tilde{b_1})$, and $(\tilde{b_2})$ states extend their speed-imposed counterparts, (i_1) and (i_2) branches are new and cannot be observed in speed control. Decreasing γ from a perfectly symmetric $(\tilde{s})$ $(\theta = 0)$ state, we can observe the asymmetry influence on temporal signals of the impeller speeds, as done in Fig. 2. First, steady states with decreasing mean θ are observed. Then [Fig. 2(b)], when $\gamma \leq -0.049$—a local extremum of the mean value of θ—small localized peaks of f_1 and f_2 are simultaneously observed, breaking time invariance. Such events are identified as excursions towards intermediate state $(\tilde{i_2})$. Still decreasing γ, the peaks grow until the biggest events saturate at low f_1 and f_2 [Fig. 2(c)]. These events are identified as transitions to the $(\tilde{b_2})$ state. For even lower values of γ, the system behavior is irregular, switching between fast $(\tilde{s})$, $(\tilde{i_2})$ and slow $(\tilde{b_2})$ states [Fig. 2(d)]. In this situation, $(\tilde{b})$ and $(\tilde{i})$ states are quasisteady, each being able to last more than 10 sec. (70 impeller rotations). Decreasing γ further affects the dynamics of the system, more time being spent in $(\tilde{b_2})$ at the expense of $(\tilde{i_2})$ and $(\tilde{s})$. Therefore, for low $\gamma \leq -0.0920$ [Fig. 2(e)], only rare events can drive the system to the faster states. Eventually, for $\gamma \leq -0.099$ [Fig. 2(f)], the system time invariance is restored, corresponding to a (b_2) steady state

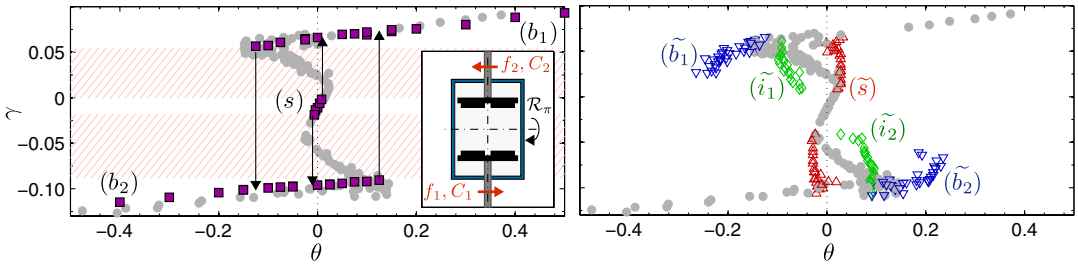

FIG. 1 (color online). (Left), mean reduced torque asymmetry γ plotted as a function of the mean reduced speed asymmetry θ, for both speed (purple squares) and torque (grey circles) experiments. The arrows indicate the possible transitions between steady states, sketching a hysteresis cycle including a forbidden γ zone (hatched region) for speed control experiments. No hysteresis is observed in torque control. (Right), modes of the θ PDF for torque control experiments corresponding to the "forbidden range." $(\tilde{s})$, $(\tilde{b_1})$, and $(\tilde{b_2})$ are quasisteady states branches extending, respectively, the steady (s), (b_1), and (b_2) branches. $(\tilde{i_1})$ and $(\tilde{i_2})$ are new branches, never observed in speed control. (Inset) Sketch of the 'VK2' experiment, with the two impellers (black). The experiment is axisymmetric along the vertical axis, and is $\mathcal{R}_\pi$ symmetric for exact counter rotation.

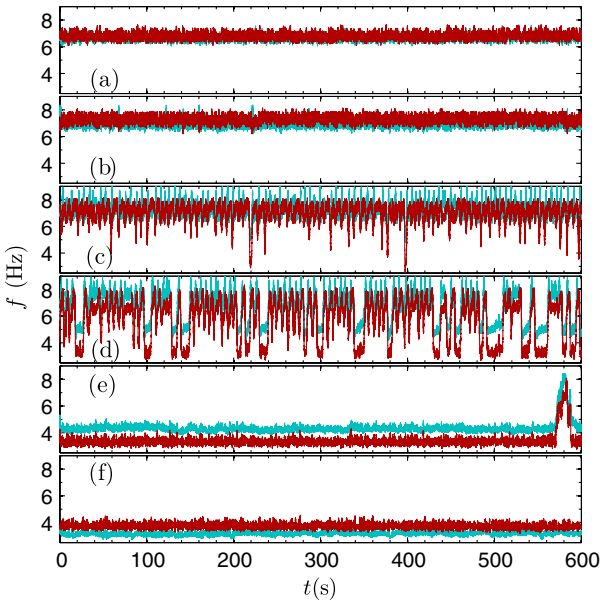

FIG. 2 (color online). Temporal series of the impeller speeds f_1 (blue) and f_2 (red) for various γ. (a), steady high-speed state $(\tilde{s})$ observed at $\gamma = -0.0164$; (b), threshold of the irregular peaks $(\tilde{i_2})$ with very small events for $\gamma = -0.0460$; (c), $(\tilde{i_2})$ irregular peaks for $\gamma = -0.0668$; (d), multistable regime showing $(\tilde{s})$, $(\tilde{i_2})$, and $(\tilde{b_2})$ events at $\gamma = -0.0891$; (e), single fast rare event in an almost steady slow $(\tilde{b_2})$ regime for $\gamma = -0.0912$; (f), steady slow (b_2) regime for $\gamma = -0.1049$.

of Fig. 1. Remarkably, the flow susceptibility defined using θ mean value, $\partial\gamma/\partial\theta$, is negative in this forbidden zone (see Fig. 1). Increasing γ from a perfectly symmetric state leads to the same sequence of events, though $(\tilde{i_1})$ and $(\tilde{b_1})$ will be reached.

Valuable information about our system dynamics can be found studying near-transition variations of global quantities [14]. We have, therefore, superposed in Fig. 3 the speed signals close to the transitions observed in Fig. 2(c): $(\tilde{s}) \rightarrow (\tilde{b_{1,2}})$ is called a down transition, and $(\tilde{b_{1,2}}) \rightarrow (\tilde{s})$ an up transition. Once the transition instant is accurately determined, a good collapse of all curves is observed, validating a unique transition path. This extends the low-dimensional system description of [14] to purely hydrodynamical quantities in a nonmagnetic turbulent flow. Eventually, the joint distributions of (f_1, f_2) are studied to highlight the attractors emerging from Figs. 1 and 2. In Fig. 4(a), for small γ, only one maximum appears, which confirms the steady nature of (s). For higher asymmetries, small excursions escaping the attractor—the previously described small $(\tilde{i_2})$ peaks—can be found, exhibiting a new local maximum strongly deviating from the diagonal $f_1 = f_2$. Still increasing the asymmetry, the system fills a large part of the (f_1, f_2) plane, with three main maxima: $(\tilde{s})$ close to the diagonal at higher (f_1, f_2), and $(\tilde{b_2})$ off diagonal for low (f_1, f_2). The third—$(\tilde{i_2})$—attractor is harder to see, being hidden by neighboring zones repeatedly crossed by

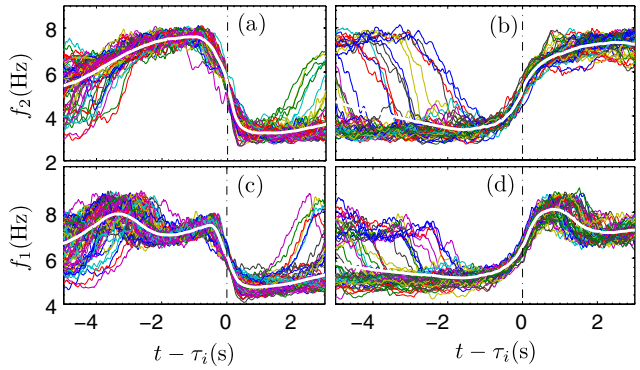

FIG. 3 (color online). Shifted temporal signals of 60 randomly chosen transitions of a two-hour experiment with $\gamma = -0.0891$. We compute τ_i by finding the minimum of $|\partial_t \tilde{f}_2|$, the 1 Hz filtered signal of f_2. (a),(c), respectively, f_2 and f_1 profiles for down transitions. (b),(d), respectively, f_2 and f_1 for up transitions. The thick white line represents in each subplot the rotation frequency averaged on all 195 events of the experiment.

unsteady events. It is located near the right tip of the histogram. With this representation, one observes a different mean path for down and up transitions: while the down transition starts "looping" next to $(\tilde{s})$ before abruptly transiting to $(\tilde{b_2})$, the up transition reaches the right tip of the joint PDF $(f_1 > f_2)$, near $(\tilde{i_2})$ before joining the $(\tilde{s})$ state.

The maxima height repartition of Figs. 4(c)–4(e) is driven by γ, from almost-fully $(\tilde{s})$, $(\tilde{i_2})$ to nearly pure $(\tilde{b_2})$ with rare, large transitions to the faster states. For nearly pure $(\tilde{s})$, we clearly see [Fig. 4(c)] a fair amount of small excursions, contrasting with the nearly pure $(\tilde{b_2})$

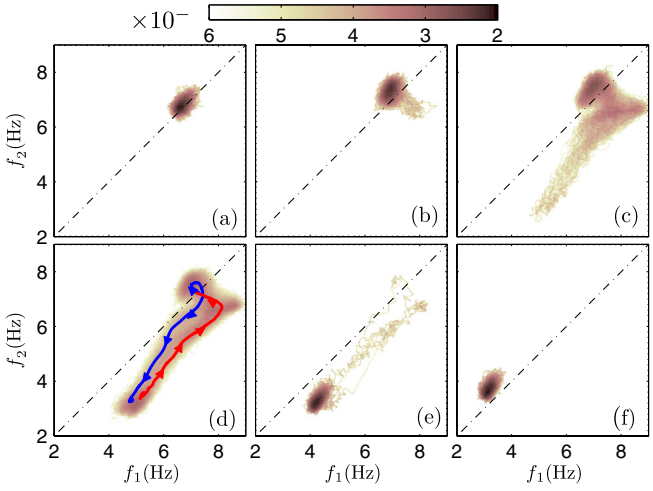

FIG. 4 (color online). Joint-probability density maps of the (f_1, f_2) values (density in log scale), based on Fig. 2 temporal series: (a): steady (s) state; (b), threshold of $(\tilde{i_1})$ events; (c), threshold of $(\tilde{b_1})$; (d), multistability: blue line and red line represent, respectively, the Fig. 3 mean profile for down and up transitions; (e), rare events; (f), steady slow state. The dashed-dotted line represents the $\theta = 0$ condition.

state [Fig. 4(e)], for which few large events are reported. The location of such maxima depends on γ: Fig. 1 recalls the γ variation of such positions. Interestingly, while the $(\tilde{b})$ and $(\tilde{s})$ abscissa increase with γ, the $(\tilde{i})$ position decreases with γ.

Discussion.—Using global torque and speed measurements, we have characterized the response of the von Kármán experiment to different energy injection mechanisms. The two responses coincide in the range of parameters accessible to speed control, reproducing the hysteresis cycle previously reported by [5]. However, imposing the torque γ in the zone inaccessible in speed control generates new continuous "mean" connections linking the symmetric (s) and bifurcated (b) branches. The mean values of the speed asymmetry θ hide the underlying phenomena observed in this forbidden zone: multiple local maxima of the PDF of θ, each corresponding to a quasisteady state, are observed. Two of them can be defined by continuity of the steady, speed-control branches: $(\tilde{s})$ and $(\tilde{b})$. The third state, $(\tilde{i})$, is never observed in any speed-imposed experiment. The study of the impellers velocity $f_1(t)$, $f_2(t)$ signals shows typical excursions and transitions between our three states, similarly to [15,16], while preliminary results on the distribution of $(\tilde{b})$ residence time favor exponential Kramers-like escape times (see Fig. 5) where the longer characteristic time increases when approaching the bifurcated (b_2) steady branch. This confirms a "potential well" interpretation of the quasisteady states as previously performed by [17].

Our results address several questions. The most striking result is the multivalued asymmetry response curve, $\gamma(\theta)$. Interestingly, other out-of-equilibrium systems also display similar multivalued characteristic curves associated with negative differential responses observed in both junction [18] and bulk electrical dipoles [19] and in vorticity-banding flows [20]. More generally, from a statistical physics point of view, the von Kármán experiment allows a quantitative analysis of the energy injection mechanism influence on the response of an out-of-equilibrium system. In that respect, negative responses are characteristic of long-range interacting systems [21], where negative specific heats $c_p = \partial u/\partial T$—another negative differential response—are allowed for equilibrium solutions in the microcanonical ensemble and forbidden in the canonical ensemble, both ensembles reaching equivalent solutions for positive specific heats. Speed control experiments are, therefore, reminiscent of canonical ensemble equilibrium solutions, torque control experiments being similar to microcanonical solutions. The dynamic multistability observed in the forbidden zone can also be seen as a probing of metastable quasisteady states due to out-of-equilibrium turbulent noise, or as temporal heterogeneities in a strongly correlated system for which no "spatial phase separation" is accepted.

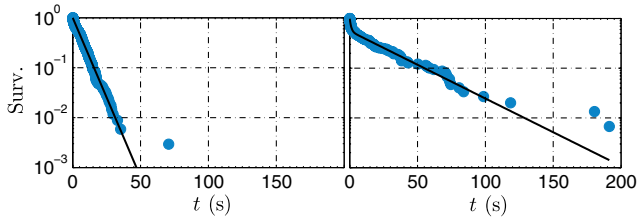

FIG. 5 (color online). Survival function $1 - \int$PDF of the distribution of the time spent in the slow quasisteady state $(\tilde{b}_1)$ before up transitions. (filled circle), experimental data; broken line, exponential fit with two characteristic times. Left, $\gamma = -0.094$ favors a simple exponential distribution. Right, $\gamma = -0.097$, closer to the edge of the steady (b_2) branch, favors separate characteristic times.

From the point of view of turbulence, the multivalued region sets the problem of universality of the steady states, that appears to be rather sensitive—at large scales—to the energy injection mechanisms, at variance with traditional views of turbulence. One interesting point to investigate is whether this sensitivity originates from the small-scale properties of the turbulent flow (therefore, breaking the universality hypothesis) or is merely a property of the larger scales. Preliminary local fluid velocity measurements (using laser Doppler anemometry) performed for $\theta = 0$ and $\gamma = 0$ have not displayed significant differences between torque and speed control on the distributions of the velocity increments. Additional and more accurate measures, in particular in the steady (b_1) and (b_2) branches and the forbidden zone, are required to fully address this important question. The phenomenon we explore in the present Letter could be present in other turbulent experimental systems: (i) in turbulent plane-Couette flows forced either with constant global stress (motor torque C) or strain (speed f); (ii) in Poiseuille flows either imposing a pressure difference, corresponding to our speed control, or a mass flow rate, equivalent to our imposed torque [22]; (iii) in Rayleigh-Bénard convection using either temperature imposed (equivalent to a constant speed) or heat-flux imposed (analogue to torque control) boundary conditions. In particular, it would be interesting to investigate the stability of the multiple steady states observed in thermal convection at very high Rayleigh numbers [23].

We thank the CNRS and CEA for support, Vincent Padilla for building the experimental device, Guillaume Mancel for sharing experimental data, and Cécile Wiertel-Gasquet for writing the acquisition programs.

*brice.saint-michel@cea.fr

[1] L. Biferale and I. Procaccia, Phys. Rep. **414**, 43 (2005).
[2] W. Thirring, Z. Phys. **235**, 339 (1970).
[3] R. S. Ellis, K. Haven, and B. Turkington, J. Stat. Phys. **101**, 999 (2000).

[4] R. Monchaux, F. Ravelet, B. Dubrulle, A. Chiffaudel, and F. Daviaud, Phys. Rev. Lett. **96**, 124502 (2006).
[5] F. Ravelet, L. Marié, A. Chiffaudel, and F. Daviaud, Phys. Rev. Lett. **93**, 164501 (2004).
[6] P.-P. Cortet, E. Herbert, A. Chiffaudel, F. Daviaud, B. Dubrulle, and V. Padilla, J. Stat. Mech. (2011), P07012; P.-P. Cortet, A. Chiffaudel, F. Daviaud, and B. Dubrulle, Phys. Rev. Lett. **105**, 214501 (2010).
[7] L. Marié and F. Daviaud, Phys. Fluids **16**, 457 (2004).
[8] J. H. Titon and O. Cadot, Phys. Fluids **15**, 625 (2003).
[9] N. Leprovost, L. Marié, and B. Dubrulle, Eur. Phys. J. B **39**, 121 (2004).
[10] S. T. Bramwell, P. C. W. Holdsworth, and J.-F. Pinton, Nature (London) **396**, 552 (1998).
[11] F. Ravelet, A. Chiffaudel, and F. Daviaud, J. Fluid Mech. **601**, 339 (2008).
[12] This range, as well as Fig. 1, does not exactly respect $\mathcal{R}_\pi$ symmetry. It is actually very difficult to obtain accurate symmetric calibrations because such experiments require small and accurate torques.
[13] B. Saint-Michel, Ph. D. thesis, Université Pierre et Marie Curie, 2013.
[14] M. Berhanu *et al.*, Europhys. Lett. **77**, 59001 (2007).
[15] F. Pétrélis and S. Fauve, J. Phys. Condens. Matter **20**, 494203 (2008).
[16] F. Pétrélis, S. Fauve, E. Dormy, and J.-P. Valet, Phys. Rev. Lett. **102**, 144503 (2009).
[17] A. de la Torre and J. Burguete, Phys. Rev. Lett. **99**, 054101 (2007).
[18] L. Esaki, Phys. Rev. **109**, 603 (1958).
[19] B. K. Ridley, Proc. Phys. Soc. London **82**, 954 (1963).
[20] D. Bonn, J. Meunier, O. Greffier, A. Al-Kahwaji, and H. Kellay, Phys. Rev. E **58**, 2115 (1998).
[21] T. Dauxois, S. Ruffo, E. Arimondo, and M. Wilkens, *Dynamics and Thermodynamics of Systems with Long Range Interactions* (Springer, New York, 2003).
[22] A. G. Darbyshire and T. Mullin, J. Fluid Mech. **289**, 83 (1995).
[23] G. Ahlers, D. Funfschilling, and E. Bodenschatz, New J. Phys. **11**, 123001 (2009).